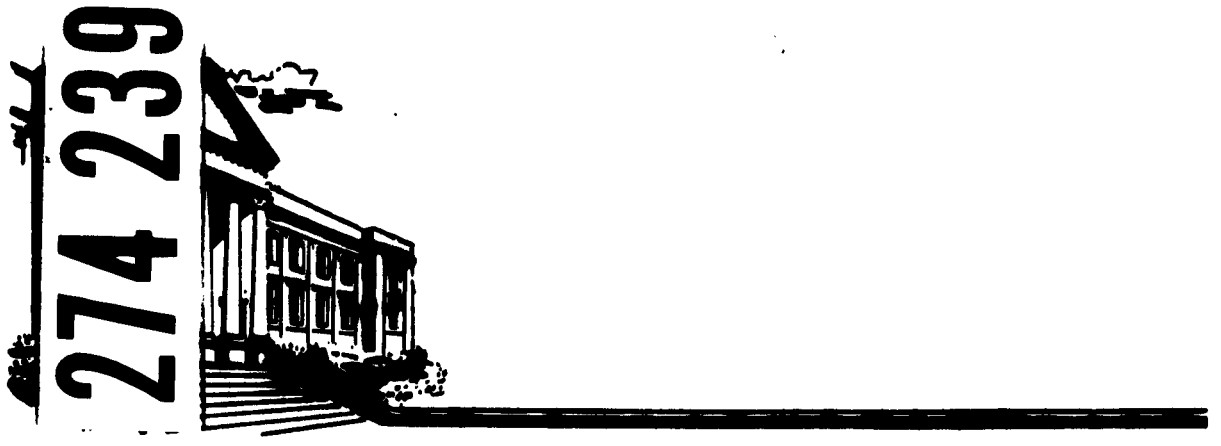

Monthly Progress Report P-B1857-7

DEVELOPMENT OF BROAD-BAND ELECTROMAGNETIC ABSORBERS FOR ELECTROEXPLOSIVE DEVICES (U)

by

Paul F. Mohrbach
Robert F. Wood

January 1 to January 31, 1962

Prepared for

U. S. NAVAL WEAPONS LABORATORY
Dahlgren, Virginia
Code WHR

NWL MIPR - 4-60
and
N178-7913

THE FRANKLIN INSTITUTE
LABORATORIES FOR RESEARCH AND DEVELOPMENT
PHILADELPHIA PENNSYLVANIA

THE FRANKLIN INSTITUTE • *Laboratories for Research and Development*

Monthly Progress Report P-B1857-7

DEVELOPMENT OF BROAD-BAND ELECTROMAGNETIC ABSORBERS FOR ELECTROEXPLOSIVE DEVICES (U)

by

Paul F. Mohrbach
Robert F. Wood

January 1, to January 31, 1962

Prepared For

U. S. NAVAL WEAPONS LABORATORY
Dahlgren, Virginia
Code WHR

NWL MIPR - 4-60

and

N178-7913

ABSTRACT

Various general methods of measuring attenuation (20 kc to 40 Mc) in a matched system are qualitatively evaluated. We have decided to use an indirect method which evaluates the attenuation from the complex voltage transfer ratio, which is relatively easy to measure.

Protective systems of interest are those offering protection against low frequency RF energy. Consideration is given to the use of electroluminescence as an energy absorber, and to photoresistive devices for protective circuits; preliminary work devising tests to investigate these approaches are noted. Further, the development of dissipative circuits is discussed. Emphasis is on defining terms and developing an approach to the problem. Analog computer studies of basic dissipative networks have begun.

To confirm or refute the assumption that high initial permeability and low volume resistivity are significant factors in the development of any low frequency ferrite attenuator, samples with extreme values of these parameters are to be obtained and measured.

Using parameters which theory indicates are prime factors in the attenuation of electromagnetic waves through a dielectric medium, we can obtain an expression which relates attenuation to frequency, permittivity, permeability, and loss tangents. This equation shows reasonable correlation with experimental data and should aid in the choice of ferrite materials.

Efforts to mold attenuators from ferrite powder are discussed.

The dielectric gap studies are concerned with the effect of capacity on attenuation. A test is discussed for determining whether reducing the center conductor area will influence attenuation.

TABLE OF CONTENTS

LIST OF FIGURES

1. INTRODUCTION

For several years, The Franklin Institute has been investigating the effect of electromagnetic radiation upon electroexplosive components. The approach has been to define the nature of the problem and then work toward a solution. From these studies has come the carbonyl iron attenuating material that can be made an integral part of the EED.

When the project was first started (October, 1956), it was felt that the RF hazard would be most acute at high frequencies. Consequently, the investigation stressed frequencies above 500 megacycles. The carbonyl iron does an adequate job in this range; it now appears, however, that the most troublesome frequencies for the Navy are around 10 megacycles and below.

The prospects of increasing the attenuation of the carbonyl iron at these frequencies is not very promising; therefore, we have shifted the major part of our research to other materials. The most promising of these materials appear to be in the ferrite families.

2. THEORETICAL AND PHYSICAL STUDIES

2.1 Determination of Sample Parameters
Contributor: Ramie H. Thompson

Since interest has recently been centered on obtaining attenuating materials in the 20 kc to 40 Mc band, it has become necessary to develop methods for determining the attenuation in matched systems of both bulk materials and "black boxes" over this frequency range. The determination of attenuation in matched systems is in keeping with our desire to quote "worst case" attenuation or more simply, true attenuation rather than insertion loss. This month's effort has been directed to evaluation of various attenuation measuring systems in this low frequency band.

2.1.1 Matched Versus Unmatched Measuring Systems

Measurement of matched-system attenuation may be approached two ways. The first and most obvious approach is to provide an impedance match at both the input and output ports, then in some way to measure the incident power and the power that gets through the attenuator. Theoretical advantages of this approach are impressive; absolute determination (i.e., we measure the actual quantities of interest) minimum calculation error and simplicity of the measurement concept. If we could construct a measurement system of this kind we would have one major problem solved. Unfortunately, the disadvantages of this system, at low frequenices, lie precisely in the difficulty of construction, and other practical considerations, involved in obtaining a matching system that will truly match the very low impedances commonly found in lossy attenuation networks.

A common and practical method of determining an impedance match is to vary the matching network until maximum power transfer is obtained; we then say we have an impedance match. This method has a serious flaw. Consider the simplified case shown in Figure 2-1, where our desire is to transfer maximum power from the generator to R_m. Let $R_G + X_G$ be fixed at any value; X_m adjustable to any [illegible], but let R_m vary only from $2R_G$ to larger values. Under these conditions a true impedance match can never occur (the reactive components can be made to cancel but the resistive components can never be equal), but if we were observing the power transferred to R_m we would definitely find a greatest value, occurring when R_m is closest to R_G (i.e., $2R_G = R_m$, the lower limit on R_G) and would still represent a 2:1 mismatch. This simplified case is fairly analogous to what occurs in an actual matching system. The losses in the matching system (which correspond to R_m in our example) cannot be made zero; therefore we cannot match impedances that have real parts smaller than the equivalent resistance of the matching system. It must be remembered that the above considerations apply

in the frequency band presently under discussion. At higher frequencies, matching systems employing coaxial elements that are almost lossless can be constructed, but even in this case large losses can occur with very low impedance devices (See FIL Report F-B1805). We do not undertake the measurement of attenuation in the 20 kc to 40 Mc band by actual measurement of power in a matched system because we cannot construct matching systems with low enough loss. This method would be usable either if the items to be measured had a large value of characteristic impedance or if the inherent losses of the matching system could be made very close to zero.

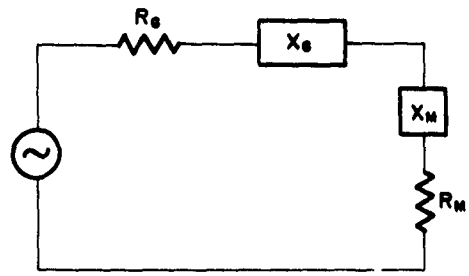

FIG. 2-1. IMPEDANCE MATCHING SYSTEM ANALOGY

The other approach to the measurement of matched attenuation is through the measurement of the electrical properties of the network, and calculation of the matched attenuation from these measurements. For lumped-parameter networks there are six similar methods of description. Each of these methods is defined in terms of the variables shown in Figure 2-2. For each method two variables are chosen to be dependent, then two equations are written for these variables in terms of the two remaining variables. The most familiar case is the impedance formulation in which the coefficients of the defining equations have the dimensions of impedance. Thus:

$$\bar{E}_1 = \bar{Z}_{11}\,\bar{I}_1 + \bar{Z}_{12}\,\bar{I}_2 \qquad (2\text{-}1)$$

$$\bar{E}_2 = \bar{Z}_{21}\,\bar{I}_1 + \bar{Z}_{22}\,\bar{I}_2 \qquad (2\text{-}2)$$

The coefficients of these equations are defined by the equations themselves by allowing first one and then the other independent variable to be zero, thus:

$$\bar{Z}_{11} \left.\frac{\bar{E}_2}{\bar{I}_1}\right|_{\bar{I}_2 = 0} \qquad \bar{Z}_{12} \left.\frac{\bar{E}_1}{\bar{I}_2}\right|_{\bar{I}_1 = 0} \tag{2-3}$$

$$\bar{Z}_{21} \left.\frac{\bar{E}_2}{\bar{I}_1}\right|_{\bar{I}_2 = 0} \qquad \bar{Z}_{22} \left.\frac{\bar{E}_2}{\bar{I}_2}\right|_{\bar{I}_1 = 0} \tag{2-4}$$

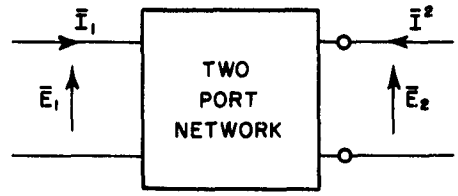

FIG.2-2. TWO PORT NETWORK VARIABLES

Modern Network Analysis by Reza and Seely (McGraw-Hill, 1959) Chap. 6, develops the above concepts and shows the interrelationship of the variously defined parameters. Chapter 7 develops the image parameters and goes on to show that the propagation constant ($\gamma = \alpha + j\beta$) of the network can be expressed (for symmetrical networks) as

$$e^{\gamma} = \bar{A} + \sqrt{\bar{A}^2 - 1} \tag{2-5}$$

where $\bar{A} = \left.\frac{\bar{E}_1}{\bar{E}_2}\right|_{\bar{I}_2 = 0}$ = open circuit voltage transfer ratio.

The attenuation constant (α) can be calculated from Eq 2-5 as

$$\alpha = \ln \left| \bar{A} + \sqrt{\bar{A}^2 - 1} \right| \tag{2-6}$$

where α is the matched attenuation of the network (db = 8.868α). We intend to base our measurements of attenuation on (Eq 2-6) since the $\bar{A}$ parameter can be readily measured at frequencies between 20 kc to 40 Mc.

We have already set up an $\bar{A}$ parameter measuring system in the range of 20 kc to 1 Mc, using an oscilloscope as the indicator of both the magnitudes and the phase separation of the input and output voltages. We intend to acquire a precision phase meter to perform phase measurements at frequencies above 1 Mc. We have a high impedance voltmeter which will measure the magnitudes of the variables from 500 kc thru 40 Mc.

There are other relationships between network parameters and the propagation constant but none more simple than Eq. 2-5. Bearing this in mind, it is doubly fortunate that the $\bar{A}$ parameter lends itself so readily to practical measurement techniques.

2.2 Protective Systems

Contributors: Norman P. Faunce and Ernst R. Schneck

Means for providing attenuation or other equally guaranteeable dissipative power loss in the frequency range of 20 kc to 10 Mc or higher is of paramount interest to this study of protective systems. A lossy transformer core material consisting of high density insulated iron powder does not appear to hold great promise to provide the magnitude of loss considered necessary. Ferrites and other not-strictly-iron core materials are being exploited for this reason, and progress in this area is discussed in Section 2.3. Studies of the feasibility of optimizing solid state phenomena as exemplified by electroluminescence and photoresistance and of developing especially lossy or particularly selective circuitry are discussed in the following.

2.2.1 Electroluminescent Studies

Electroluminescent phosphors are of interest as a possible means of energy absorption. A phosphor of zinc oxide and copper activated zinc sulfide is of interest because its possible electrical energy absorbing characteristics appear to be very good.

Equipment necessary for the preparation of this phosphor, at a temperature of 1200°C in the presence of an inert atmosphere, is being made ready. A Vycor ground glass joint was obtained, and fixed to the quartz tube (oven core) container. However, the outer Vycor member cracked when being fitted with the necessary attachments. This misfortune is rare with Vycor, and was thought to result from thermal stresses developed during working. Another glass member was ordered, and we are awaiting the fitting of the member with the necessary attachments. Barring further unforeseen delays, our examination of the phosphor should begin within the next period.

2.2.2 Photoresitive Devices

Devices such as photoresistors and photoresistor switches are under study for possible use in protective networks. Photoresistors (and photoresistor switches with enclosed light source) vary their resistance when exposed to light; this property may enable their use in protective circuitry to block unwanted stimuli. Under a complementary program we obtained several of these elements. Tests of these items with electrical stimuli have pointed out several problem areas with respect to their use, chief of which are low power handling capabilities and capacitive coupling at the megacycle frequencies.

One such device tested consisted of an encapsulated filament light source and photoresistor. Our hope was that the characteristics of light and resistance would combine to make the unit respond nonlinearly with respect to frequency. Tests indicate this was not the case, since the filament responds as well to the higher audio frequencies as to dc. Such commercially available photoresistor switches, therefore, seem impractical for any application to our problem.

Recently we received an electroluminescent panel which produces red light, the color to which many photoresistors are most sensitive. We

shall examine this device both by itself, and in conjunction with photo-resistor devices for desirable electrical response characteristics.

2.2.3 Dissipative Network Development

A dissipative network to provide 30 db of "terminated power loss" (TPL)[1] for frequencies of 20 kc to 1 Mc or higher, yet limited to 3 db for the dc to 10 kc range, is the design objective of this phase of study. The achievement of this goal is being expedited by enlisting the aid of an analog computer to perform the otherwise tedious computations.

Included in Appendix B of this report is a discussion of the analog program, which shows the form which the analytical procedure will take. Though the final network will most probably consist of a series of "L" sections not of equal component value, we plan to first concentrate on equal-valued repeating sections. Our preliminary investigations will be confined to exploring the limit to which we may go with a single basic network.

Appendix A shows the development of the TPL ratio for an n-compounded constant-impedance network. As indicated in this discussion, the proper choice of parameter values yields a network that makes for relatively easy hand calculation of TPLR. The analog program will be designed to disregard this simplification so as to handle the more complex problem; thus, this easy problem for hand calculation will be as difficult for the machine as any we may desire to give to it. Consequently the development of Appendix A gives us a means for checking the analog program in simple fashion.

During this period we have made a few preliminary runs with the analog program. These were primarily check-out and debugging exercises. Most of our troubles have been resolved so that we should be

---

[1] Terminated Power Loss the power loss (apparent attenuation) inherent in a terminated (one-port) network. See Appendix A.

operating on our planned program during the next period. Our first large scale analyses will be directed toward examining the effect on the TPLR vs frequency characteristic for the network shown in Figure A-1 for changes in any one of the four basic parameters. The subsequent steps to be taken will depend upon the analysis of these preliminary data.

2.3 Evaluation of Ferrites

Contributors: Harvey P. Goldberg and Daniel J. Mullen

Ferrites have been shown to possess properties which make them particularly attractive for use as RF attenuators at frequencies below 500 Mc. Samples of several ferrites have been obtained and preliminary data have been reported that supports this view.

There are two preliminary phases in this program of ferrite evaluation. The first is the obtaining of special toroids made to the dimensions of our carbonyl iron plugs, so that they can be measured in our immittance bridge measuring system. The choice of the ferrite is made according to our analysis of those electrical and magnetic properties which appear to be significant. An equation has been derived theoretically which defines attenuation as a function of frequency, complex permeability and complex permittivity. Calculations using this equation have shown reasonable correlation with actual measurements and, therefore, by proper manipulation of this equation, it is expected that a suitable choice of properties can be made to obtain the largest attenuation through a range of frequencies. Arrangements have been made to obtain several commercial ferrites, so that this aspect of the program can be continued.

The second phase is the molding of ferrites from raw ferrite powders which we have on hand. The object here in this phase is to find out if fired ferrite powder can be molded and subsequently treated to yield an assembly with the necessary mechanical strength and reasonable attenuation.

It is our hope that this approach will eventually lead to a controlled program of ferrite development in which specifications can be set that will produce an end product fulfilling our present requirements.

2.3.1 Attenuation Measurements of Ferrite Materials

According to our analysis of electrical and magnetic properties of ferrites, which are significant in the development of a low frequency RF attenuator, a high initial permeability and low volume resistivity are most likely to afford maximum energy loss if used to the fullest advantage. To prove the validity of these original assumptions high initial permeability and low volume resistivity, we are asking for samples (from three separate manufacturers) which have extreme values of these properties. Upon receipt of these samples, we shall evaluate them.

2.3.2 Theoretical Approach to the Problem of Attenuation at Low Frequency

Last month an expression relating attenuation to frequency, complex permittivity, and complex permeability was given as follows:

$$\alpha = \frac{\omega}{\sqrt{2}}\sqrt{\mu_0 \epsilon_0}\left[-(\epsilon''\mu''-\epsilon'\mu') + \sqrt{\epsilon'^2\mu'^2+\epsilon''^2\mu''^2+\epsilon''^2\mu'^2+\epsilon'^2\mu''^2}\right]^{\frac{1}{2}} \text{ neper/meter} \qquad (2\text{-}7)$$

This deviation actually defined $(-\gamma)$, and also implicity assumes that μ'' and ϵ'' are negative real numbers. Introduction of minus signs of μ'' and ϵ'' does not change the form of the equation. To express γ as a positive quantity, we may factor a minus sign outside of the bracket, and we have

$$-\alpha = \frac{\omega}{\sqrt{2}}\sqrt{\mu_0 \epsilon_0}\left[+(\epsilon''\mu''-\epsilon'\mu') - \sqrt{\epsilon'^2\mu'^2+\epsilon''^2\mu''^2+\epsilon''^2\mu'^2+\epsilon'^2\mu''^2}\right]^{\frac{1}{2}} \text{ neper/meter} \qquad (2\text{-}8)$$

This minus α corresponds to the real part of the propagation constant γ if the negative root is taken of the radical inside the bracket. Therefore we can write

$$\mathrm{re}\ (\gamma) = \alpha = \frac{\omega}{\sqrt{2}}\sqrt{\mu_o \epsilon_o}\left[+(\epsilon'' \mu'' - \epsilon' \mu') + \sqrt{\epsilon'^2 \mu'^2 + \epsilon''^2 \mu''^2 + \epsilon''^2 \mu'^2 + \epsilon'^2 \mu''^2}\right]^{\frac{1}{2}} \text{ neper/meter} \tag{2-9}$$

From now on, our reports will use α as defined in Equation 2-9 and $\gamma = \alpha + j\beta$ where both α and β are positive real numbers.

Referring to Equation 2-2 in last month's report, it is apparent that ϵ', ϵ'', μ', and μ'' are defined as the relative parts of complex permittivity and complex permeability. To avoid confusion we shall let

$$k'_\epsilon = \epsilon' \text{ (relative)}$$
$$k''_\epsilon = \epsilon'' \text{ (relative)}$$
$$k'_\mu = \mu' \text{ (relative)}$$
$$k''_\mu = \mu'' \text{ (relative)}$$

Therefore equation 2-9 can be rewritten:

$$\alpha = \frac{\omega}{\sqrt{2}}\sqrt{\mu_o \epsilon_o}\left[(k''_\epsilon k''_\mu - k'_\epsilon k'_\mu) + \sqrt{k'^2_\epsilon k'^2_\mu + k''^2_\epsilon k''^2_\mu + k''^2_\epsilon k'^2_\mu + k'^2_\epsilon k''^2_\mu}\right]^{\frac{1}{2}} \text{ neper/meter} \tag{2-10}$$

This equation can be rearranged further by dividing out $k'_\epsilon k'_\mu$ inside the bracket and remembering that $\tan \delta_\epsilon = \frac{k''_\epsilon}{k'_\epsilon}$ and $\tan \delta_\mu = \frac{k''_\mu}{k'_\mu}$ we have

$$\alpha = \frac{\omega}{\sqrt{2}}\sqrt{\mu_o \epsilon_o}\left\{k'_\epsilon k'_\mu \left[(\tan \delta_\epsilon \tan \delta_\mu - 1) + \sqrt{1 + \tan^2 \delta_\epsilon \tan^2 \delta_\mu + \tan^2 \delta_\epsilon + \tan^2 \delta_\mu}\right]\right\}^{\frac{1}{2}} \text{ neper/meter} \tag{2-11}$$

The more convenient units of decibels can be substituted for nepers in equation 2-11 by employing the conversion factor

$$1 \text{ neper} = 8.686 \text{ db.} \tag{2-12}$$

$$\alpha = 1.28 \times 10^{-9} f \left\{ k_\epsilon^1 k_\mu^1 \left[(\tan\delta_\epsilon \tan\delta_\mu - 1) + \sqrt{1+\tan^2\delta_\epsilon \tan^2\delta_\mu + \tan^2\delta_\epsilon + \tan^2\delta_\mu} \right] \right\}^{\frac{1}{2}} \text{ db/cm} \tag{2-13}$$

The relative permittivity, relative permeability, and loss tangents may be combined into one variable, A, which is

$$A = \left\{ k_\epsilon^1 k_\mu^1 \left[(\tan\delta_\epsilon \tan\delta_\mu - 1) + \sqrt{1+\tan^2\delta_\epsilon \tan^2\delta_\mu + \tan^2\delta_\epsilon + \tan^2\delta_\mu} \right] \right\} \tag{2-14}$$

A final equation

$$\alpha = 1.28 \times 10^{-9} \; f \; [A]^{\frac{1}{2}} \text{ db/cm} \tag{2-15}$$

is obtained in which α can be plotted as a function of A and frequency. A family of these curves is shown in Figure 2-3. At low frequencies, the magnitude of A must be large to produce an appreciable amount of attenuation. "A", however, is directly proportional to the square roots of the relative permittivity and relative permeability, and to the loss tangents in a more complex manner. Therefore materials with large relative permittivities, relative permeabilities and loss tangents should possess higher attenuation at low frequencies.

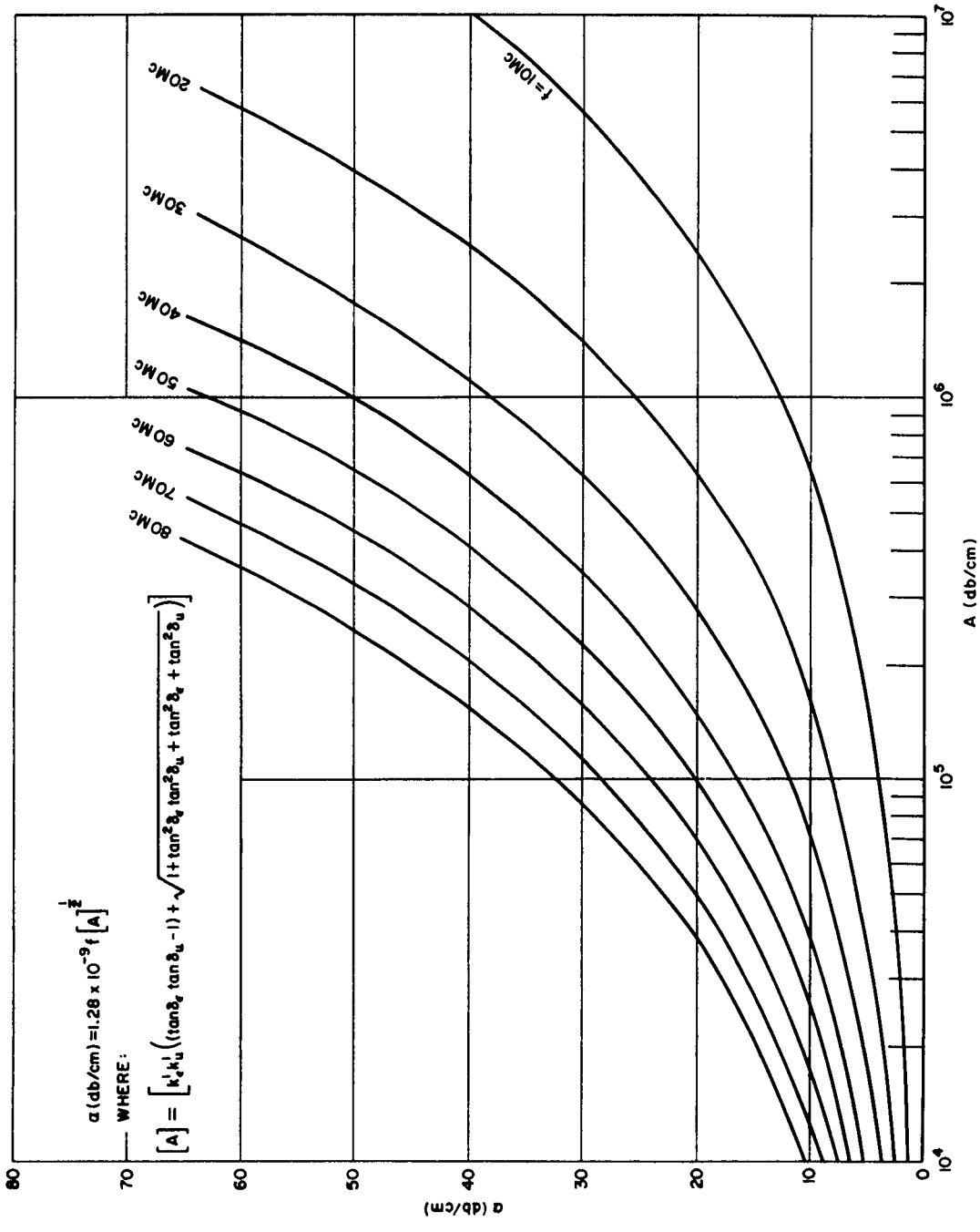

FIG 2-3 THEORETICAL ATTENUATION CURVE WITH FREQUENCY AS A PARAMETER

2.3.3 Molding of Ferrite Powders

Initial efforts to produce attenuators from ferrite powders have been resulting in poor mechanical strength. To overcome this defect, we added an epoxy binder to the samples. The epoxy content of the sample was varied from 5% to 20%. The mechanical strength and resilience of the samples were vastly improved. The attenuation was approximately 3 db per sample at 500 Mc and did not vary appreciably with epoxy content.

Our next step was to substitute a material having a high dielectric constant for the epoxy. TiO_2 and $BaTiO_3$ were used in concentrations of 5% and 10%. In our previous work, with carbonyl iron powder as the attenuating material, it was noticed that the inclusion of these materials increased the attenuation of the samples. However, when samples were pressed from $BaTiO_3$ and TiO_2 ferrite mixtures, they were still very weak. Some samples were enclosed in brass bands and heated to 250°C to produce a partial sintering effect. Results obtained for these were rather erratic and difficult to reproduce. The attenuation of the samples at 500 Mc varied from 2.5 db per plug to 5 db per plug and the dc resistance of the attenuators varied from 500 ohms to 10,000 ohms.

These experiments led us to conclude that sintering would probably be necessary to achieve the sought-for mechanical strength. However, we still had the problem of the samples crumbling when no binder was used. We decided to try etching the powder to improve its cohesion when pressed into a toroid configuration. The powder was immersed in a solution of 5% HNO_3 for two hours, then washed with distilled water and dried in an oven at 130°C. Samples fabricated in this manner were strong enough to hold up under the sintering procedure.

A standard industrial procedure for temporarily holding ferrite powders together prior to sintering is the use of water as a binder.

Water is used because it will evaporate during the sintering operation and leave no residual contaminants. Exploring this technique we found that one drop of water per gram of ferrite powder is quite sufficient to enable us to sinter our samples. These samples, having water as a binder, are placed in an oven at 350° for five or six hours. This treatment improves the mechanical strength of our samples but does not alter attenuation. However, to obtain a truly sintered sample we will need temperatures of 1000°C to 1400°C. We are therefore considering the use of high temperature ovens or an induction heater for high temperature sintering of ferrite powders. These possibilities will be explored more fully during the next month.

3. CHEMICAL STUDY

No work has been done on this phase during the past report period.

4. APPLIED STUDIES

4.1 Dielectric Gap Study
Contributor: James D. Dunfee

The insertion of a high dielectric between an attenuating material and the conductors is desirable to increase both the dielectric strength of the attenuator and the dc resistance. Several of the lossy attenuating materials that are presently being investigated have fairly low dielectric strength and low dc resistance.

During the past year, our efforts have been directed toward proving the theory that a thin layer of a high dielectric can be placed between a conductor and a lossy material without affecting the material's RF attenuation characteristic. Curves have been presented showing the relationship between material thickness, its dielectric constant, and the change in RF attenuation of an insulated attenuator from that of an uninsulated attenuating material. Most of the data were obtained using

ceramic insulating materials, at a test frequency of 500 megacycles. Work at lower frequencies gave results similar to that obtained at 500 megacycles; i.e. the same percentage of attenuation was lost.

Recently, we measured the capacity of our assemblies, and plotted this parameter versus the loss in attenuation over non-insulated assemblies. Increasing the capacity of the insulating material reduced this attenuation loss. Since decreasing the material thickness and raising the dielectric constant gave the same result, this appeared first, to be a simple data correlation. But, capacity can also be changed by varying the effective area of the capacitor plates. By silvering the insulating material that extends past the ends of the carbonyl iron doughnut which increases the capacity between conductors we have been able to realize the full attenuation of the lossy material when using a lower K insulator.

Data indicate that reducing the center conductor diameter, (thereby reducing the capacity), would require an increase in the dielectric constant to obtain full attenuation with a given thickness of material. Though we have no reason to expect anything different, we are now designing a test to prove this point. Conceivably, with such data on hand, we will then be in a position to specify and select a suitable material for placement between the conductors and the lossy material to give full attenuation and also high voltage breakdown insulation between conductors. Application of a film of this material to the conductors can then be attempted.

5. CONCLUSIONS AND FUTURE PLANS

Matched attenuation is to be evaluated in the 20 kc to 40 Mc frequency band by measurement of the complex open circuit voltage transfer ratio. One measurement system of this type covering 20 kc to 1 Mc is already operational. The Laboratories are purchasing a Model 205A1 phase meter (Ad-Yu Electronics Lab., Inc.) which should be delivered in three weeks. This will permit us to make attenuation measurements up to 40 Mc. From 40 Mc to 500 Mc we are investigating the use of the General Radio admittance bridge for attenuation measurements. The range

of 200 Mc to 10,000 Mc is already covered by a matching system using double-stub tuners.

Other parametric methods for evaluating attenuation have not been abandoned; some will be used as cross checks on our present system and others are still under study.

Studies in protective systems have concerned themselves with preparations for electroluminescent phosphor evaluation, the search and obtaining of commercially available electroluminescent and photoresistive devices and with preliminary tests of the latter. Preparation for future examination of dissipative networks by an analog computor will depend on analysis of preliminary results to be available during the next period.

Upon receipt of special ferrite toroids, the program of attenuation measurement will be continued.

Further work will be done with the equations with the view of predicting from them what the relationship of permittivity, permeability and loss tangents is with respect to attenuation and how it can be optimized.

It appears that samples made from powdered ferrite will require sintering in order to obtain a sample with a good mechanical strength. For sintering, temperatures of 1000°C to 1400°C are needed; therefore, consideration will be given to the use of high temperature ovens or an induction heater.

Next month we plan to formulate a moldable low K dielectric in an effort to obtain large diameters suitable for placement between the outer conductor and the carbonyl iron doughnut. Such a configuration would be suitable for coaxial devices. The large area available should increase the capacity of a thin layer of low K dielectric sufficiently to minimize the loss in attenuation.

We have available some high dielectric samples (K of 1200) measuring about 1/16 in. OD x 1/32 in. ID x 1/8 in. long. This should help to provide an interesting correlation or extension of our present theories relating capacity and dielectric constant versus attenuation loss.

P. F. Mohrbach
Project Leader

Approved by:

E. E. Hannum, Manager
Applied Physics Laboratory

Francis L. Jackson
Director of Laboratories

APPENDIX A
(Contributor Norman P. Faunce)

THE TERMINATED POWER LOSS FOR AN N-COMPOUNDED CONSTANT-IMPEDANCE NETWORK

We are interested in protecting the bridge wires of electro-explosive initiators from receiving RF energy. One approach is to incorporate within the casing (shield) of the EED a dissipative filter between the bridgewire and the electrodes (firing leads). In evaluating such filters we are mainly interested in how much power they will prevent from reaching the bridgewire. To analyze such devices we can consider a four terminal network containing dissipative elements with a dissipative termination or load which corresponds to the bridgewire. The power dissipated in the network (TPL) for a given load termination (bridgewire) is a measure of the effectiveness of the device as an RF attenuator.

Any terminated four terminal network containing dissipative elements (other than the termination) will have associated with it a unique minimum power loss characteristic dependent upon the parameters of the specific network. Neither an attenuation constant nor an insertion loss ratio will serve to clearly define this characteristic, but instead a new network constant, "Terminated Power Loss" (TPL) must be defined.

If P_n represents the amount of power dissipated by the total network including the termination and P_o is the amount of the power dissipated by the termination or load, then the Terminated Power Loss is given by:

$$TPL = 10 \text{ Log}_{10} \frac{P_n}{P_o} \quad \text{(db)} \qquad \text{(A-1)}$$

Terminated Power Loss Ratio (TPLR) is simply $\frac{P_n}{P_o}$. For the network shown in Figure A-1, the complex power may be characterized by the

product $\bar{E}\,\bar{I}^*$. The power dissipated by the total network will be $\bar{E}\ \bar{I}\ \cos\theta$ where θ is the phase angle of the network's input impedance. However, P_n may be equally well determined by summing the power dissipated by both R_n and R_o. If R_o is taken as the termination then,

$$TPLR = \frac{P_{R_o} + P_{R_n}}{P_{R_o}} = 1 + \frac{P_{R_n}}{P_{R_o}} \qquad (A\text{-}2)$$

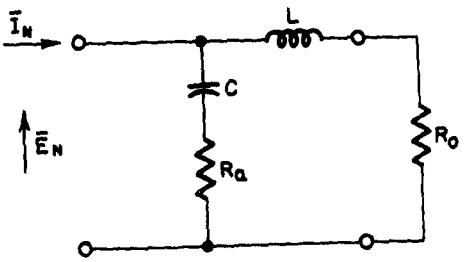

FIG. A-1. BASIC DISSIPATIVE NETWORK

The power dissipated in a resistive component is given by

$$P_R = \frac{\left|\bar{E}_R\right|^2}{R} \qquad (A\text{-}3)$$

Substituting (A-3) into (A-2)

$$TPLR = 1 + \frac{\left|\bar{E}_{R_n}\right|^2 \quad R_o}{\left|\bar{E}_{R_o}\right|^2 \quad R_n} \qquad (A\text{-}4)$$

A simplified expansion for $\left|\bar{E}_{R_n}\right|^2$ and $\left|\bar{E}_{R_o}\right|^2$ can be obtained by looking at Figure A-1. In the capacitive branch the total impedance is

$$\bar{Z}_c = R_n + \frac{1}{j\omega C} \qquad (A\text{-}5)$$

Total current in this branch is $\bar{I}_{t_c} = \dfrac{\bar{E}_n}{\bar{Z}_c}$ and the voltage across the resistor R_n is therefore (A-6)

$$\bar{E}_{R_n} = \bar{I}_{t_c} R_n = \frac{\bar{E}_n}{\bar{Z}_c} R_n \qquad \text{(A-7)}$$

$$\bar{E}_{R_n} = \frac{\bar{E}_n R_n}{R_n + \frac{1}{j\omega c}} \qquad \text{(A-8)}$$

With a little manipulation the magnitude squared of equation (A-8) can be shown to be

$$\left|\bar{E}_{R_n}\right|^2 = \frac{\left|E_n\right|^2}{1 + Q_c^2} \quad \text{where } Q_c = \frac{1}{\omega C R_n} \qquad \text{(A-9)}$$

In a like manner $\left(\left|\bar{E}_{R_o}\right|^2\right)$ can be expressed as

$$\left|\bar{E}_{R_o}\right|^2 = \frac{\left|E_n\right|^2}{1 + Q_L^2} \quad \text{where } Q_L = \frac{\omega L}{R_o} \qquad \text{(A-10)}$$

To obtain a constant input impedance at all frequencies, the following condition must be satisfied[1]

$$R_o = R_n = R = \sqrt{L/C} \qquad \text{(A-11)}$$

This results in a purely resistive circuit and, therefore a unity power factor.

Combining (A-9) and (A-10) with (A-4) yields the final result:

$$\text{TPLR} = 1 + Q_L^2 = 1 + \frac{1}{Q_C^2} \qquad \text{(A-12)}$$

---

[1] John D. Ryder, Networks, Lines, and Fields (Englewood Cliffs, New Jersey, Prentice-Hall, Inc., 1959), p. 76.

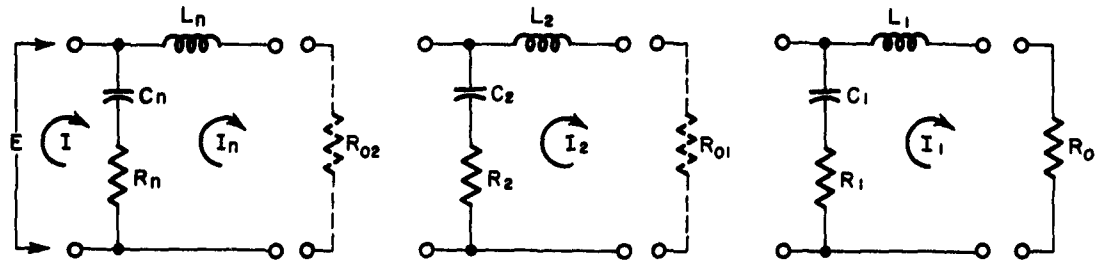

FIG. A-2. N-COMPOUNDED CONSTANT RESISTANCE NETWORK

This expression defines the power loss for the last section of the repetitive network shown in Figure A-2. However, this network consisting of L_1, C_1, R_1, and R_o, when terminating the second section can be represented by a resistance $R_{01} = R_0$. Likewise, the second section when terminated by the first can be constructed to be equivalent to an R_{02} terminating a third or nth section.

The terminated power loss ratio for the n-th section is

$$TPLR_n = 1 + Q_{L_n}^2 \tag{A-13}$$

and the total loss ratio will be the product of the individual loss ratio

$$TPLR_T = \left[1 + Q_{L_1}^2\right] \left[1 + Q_{L_2}^2\right] \text{--------} \left[1 + Q_{L_n}^2\right] \tag{A-14}$$

Making the additional restriction that $L_1 = L_2$ and $C_1 = C_2 = C_n$ further simplifies this to:

$$TPLR_T = \left[1 + Q_{L_n}^2\right]^n \tag{A-15}$$

$$TPL_T = 10n \ \text{Log}_{10}\left[1 + Q_{L_n}^2\right] \tag{A-16}$$

APPENDIX B
(Contributor Edward W. Jones)

INTRODUCTION

The dissipative networks being investigated by the analog computer will consist of "L" sections as shown in Figure A-2. The response of the network to various input voltage functions such as rectangular pulses, condenser discharges, and sine waves of various frequencies etc. is of interest. Of particular interest is the terminated power loss ratio, which is defined by:

$$TPLR = \frac{Pin(Re)}{Pout(Re)} \qquad \text{(B-1)}$$

where TPLR = Terminated Power Loss Ratio

Pin(Re) = Real Power Input to Network in Watts

Pout(Re)= Real Power Dissipated in the Output Resistor R_o in watts

as the frequency of a sinusoidal driving voltage to the network is varied. The computation will be performed on an electronic analog computer which will solve the differential equations associated with the network; each loop of the network requires one second order linear differential equation with constant coefficients to describe its behavior. Regardless of their physical nature, the variables being studied by means of an electronic analog computer are each represented by a voltage proportional to the variable. Thus, in this case, voltages,currents, powers, etc., at any point in the circuit being investigated will be represented by a voltage somewhere in the analog computer circuits. The computer voltage representing a given variable is converted to the physical system variable by means of a scale factor. Scale factors are established when the problem is programmed for the computer.

MATHEMATICAL ANALYSIS OF THE PHYSICAL SYSTEM CIRCUITS

The first circuit to be considered is a single "L" section feeding into R_o and fed from a voltage source of a value E. The current in the loop containing R_o (as seen in Figure A-2) is I_1 and the current through the voltage source (which is equal to the total current into the network in all cases) is I. On writing differential equations for the two loops we arrive at:

$$E - \frac{1}{C_1}\int_o^t (I - I_1)\, dt - R_1 (I - I_1) = 0 \qquad \text{(B-2)}$$

$$R_1(I_1 - I) + \frac{1}{C_1}\int_o^t (I_1 - I)\, dt + L_1 \frac{dI_1}{dt} + R_o I_1 = 0 \qquad \text{(B-3)}$$

Solving the first equation for I and the second for $\frac{dI_1}{dt}$ we have:

$$I = \frac{E}{R_1} - \frac{1}{R_1 C_1}\int_o^t (I - I_1)\, dt + I_1 \qquad \text{(B-4)}$$

$$\frac{dI_1}{dt} = \frac{R_1}{L_1}(I - I_1) + \frac{1}{L_1 C_1}\int_o^t (I - I_1)\, dt - \frac{Ro}{L_1} I_1 \qquad \text{(B-5)}$$

These are the differential equations of the physical system. As they now stand these equations would be difficult to solve on an analog computer because they require impractically high amplifier gains. In addition to that, the physical system phenomena take place so rapidly that available recording instruments do not have adequate response speed. These difficulties can be overcome by a change in time scale. We therefore let:

$$t = \beta \tau \tag{B-6}$$

from which $dt = \beta d\tau$ (B-7)

where t = Real (Physical System) Time

τ = Computer Time

β = Time Scale Factor

On replacing dt in the above equations by $\beta d\tau$ we obtain, after a little manipulation:

$$I = \frac{\bar{E}}{R_1} - \frac{\beta}{R_1 C_1}\int_o^\tau (I-I_1)\, d\tau + I_1 \tag{B-8}$$

$$\frac{dI_1}{d\tau} = \frac{\beta R_1}{L_1}(I-I_1) + \frac{\beta^2}{L_1 C_1}\int_o^\tau (I-I_1)d\tau - \frac{\beta R_o}{L_1} I_1 \tag{B-9}$$

In the same way we can write the general differential equation for the n-th loop (n>1) as:

$$\frac{dI_n}{dt} = \frac{\beta R_n}{L_n}(I_{n+1} - I_n) + \frac{\beta^2}{L_n C_n}\int_o^\tau (I_{n+1}-I_n)d\tau + \frac{\beta^2}{L_n C_{n-1}}\int_o^\tau (I_{n-1} - I_n)\, d\tau + \frac{\beta R_{n-1}}{L_n}(I_{n-1}-I_n) \tag{B-10}$$

DISTRIBUTION LIST

Commander(5)
U.S. Naval Weapons Laboratory
Dahlgren, Virginia
Attn: Code WHR, Lyde Pruett

Office of Naval Research
University of Pennsylvania
Rm. 213, Hare Building
Philadelphia 4, Penna.
Attn: Mr. R. L. Keane

Chief, Bureau of Medicine and Surgery
Department of the Navy
Washington 25, D. C.
Attn: Code 74

Chief, Bureau of Yards & Docks
Department of the Navy
Washington 25, D. C.

Commander
U.S. Naval Ordnance Laboratory
White Oak, Maryland
Code: ED
NO
LV
Technical Library

Commander
U.S. Naval Ordnance Test Station
China Lake, California
Code: 556
4572

Officer-in-Charge
U.S. Naval Explosive Ordnance Disposal Technical Center
U.S. Naval Propellant Plant
Indian Head, Maryland

Commandant of the Marine Corps
Washington 25, D. C.
Code: AO4C

Contracting Officer
U.S. Naval Weapons Laboratory
Dahlgren, Virginia
Attn: Code SSCP

Chief, Bureau of Naval Weapons
Department of the Navy
Washington 25, D. C.
Code: C-132
RM-15
RMMO-224
RMMO-235
RMMO-32
RMMO-33
RMMO-4
RMMO-43
RMMO-44
RMMP-343
RREN-32
DLI-31

Commanding Officer
U.S. Naval Ordnance Laboratory
Corona, California
Code: 561
552

Commanding Officer
U.S. Naval Air Development Center
Johnsville, Penna.
Code: EL-94

Commanding Officer
U.S. Naval Underwater Ordnance Station
Newport, Rhode Island

Director
U.S. Naval Research Laboratory
Washington 25, D. C.
Code: 5439 (1)
5410 (2)

DISTRIBUTION LIST (Continued)

Commander
Pacific Missile Range
P. O. Box 8
Point Mugu, California
Attn: Code 3260

Commanding Officer
U.S. Naval Ordnance Plant
Macon, Georgia
Attn: Code PD 270

Commander Service Force
U.S. Atlantic Fleet
Building 142, Naval Base
Norfolk 11, Virginia

Commanding General
Headquarters, Fleet Marine Force,
Pacific
c/o Fleet Post Office
San Francisco, California

Commander
Philadelphia Naval Shipyard
Naval Base
Philadelphia 12, Penna.
Code 273

Commander
Pearl Harbor Naval Shipyard
Navy No. 128, Fleet Post Office
San Francisco, California
Code 280

Office Chief Signal Officer
Research and Development Division
Washington 25, D. C.
Attn: SIGRD-8

Commanding Officer
Diamond Ordnance Fuze Laboratories
Washington 25, D. C.
Attn: William Binkley,
Code 420

Commanding Officer and Director
U.S. Navy Electronics Laboratory
San Diego 52, California
Attn: Library

Commander Naval Air Force
U.S. Atlantic Fleet (CNAL 724B)
U.S. Naval Air Station
Norfolk 11, Virginia

Commander Training Command
U.S. Pacific Fleet
c/o U.S. Fleet Anti-Submarine
Warfare School
San Diego 47, California

Commander in Chief
c/o Fleet Post Office
San Francisco, California

Commander
New York Naval Shipyard
Weapons Division,
Naval Base
Brooklyn 1, New York
Attn: Code 290
Code 912B

Commander
Portsmouth Naval Shipyard
Portsmouth, New Hampshire

Department of the Army
Office Chief of Ordnance
Washington 25, D. C.
Attn: ORDGU-SA
ORDTN

U.S. Army Nuclear Weapon Co-
ordination Group
Fort Belvoir,
Virginia

DISTRIBUTION LIST (Continued)

Director
U.S. Army Engineer Research and Dev. Labs.
Fort Belvoir, Virginia
Attn: Chief, Basic Research Group

Commanding Officer
U.S. Army Environmental Health Laboratory
Building 1235
Army Chemical Center, Maryland

Commanding General
Headquarters 2DRAADCOM
Oklahoma City AFS,
Oklahoma City, Okla.

Commander
U.S. Army Ordnance
Frankford Arsenal
Philadelphia 37, Pa.

Commanding Officer
Office of Ordnance Research, U.S. Army
Box CM, Duke Station
Durham, North Carolina
Attn: Internal Research Division

Commanding Officer(4)
White Sands Missile Range, New Mexico
U.S.A. SMSA
Attn: SIGWS-AJ

Director of Office of Special Weapons Developments
United States Continental Army Command
Fort Bliss, Texas
Attn: Capt. Chester I. Peterson
T S Control Officer

Commanding Officer
Picatinny Arsenal
Dover, New Jersey
Attn: Artillery Ammunition & Rocket Dev.
Laboratory - Mr. S. M. Adelman
Attn: Mr. Abraham Grinoch, Chief
Evaluation Unit,
Instrumentation Section,
Bldg. 352

Commanding Officer
U.S. Army Signal Research and Development Laboratory
Fort Monmouth, New Jersey
Attn: SIGEM/EL-GF

Commander
U.S. Army Rocket and Guided Missile Agency
Redstone Arsenal, Alabama
Attn: ORDXR-R (Plans)

Commanding General
White Sands Missile Range
New Mexico
Attn: ORDBS-G3

Commanding General
U.S. Army Electronic Proving Ground
Technical Library
Ft. Huachuca, Arizona

Headquarters
Air Force Systems Command
Andrews Air Force Base
Washington 25, D. C.
Attn: SCIZM

Commander
Air Force Missile Test Center
Patrick Air Force Base, Florida
Code MTRCF

DISTRIBUTION LIST (Continued)

Headquarters
Ogden Air Material Area
Hill Air Force Base
Ogden, Utah
Code OOYSS

Griffiss AF Base
RADC, New York
Attn: RCLS/Philip L. Sandler

Commanding General
Air Fleet Marine Force, Pacific
MCAS, El Toro
Santa Ana, California

Armed Services Explosives Safety Board
Department of Defense
Room 2075, Bldg. T-7, Gravelly Point
Washington 25, D. C.

Commander
Field Command
Defense Atomic Support Agency
Albuquerque, New Mexico
Attn: FCDR3

U.S. Atomic Energy Commission
Division of Military Application
Washington 25, D. C.

American Machine & Foundry Co.
Alexandria Div.
1025 North Royal St.
Alexandria, Va.
Attn: Dr. L.F. Dytrt
(Contract AF-29(601)-2769)

Convair
Division of General Dynamics Corp.
Pamona, California
Attn: Division Library

Deputy Inspection General for Safety (AFIGS-B)
Norton Air Force Base,
California

Commander
Charleston Naval Shipyard
U.S. Naval Base
Charleston, South Carolina

Commander
Air Force Special Weapons Center
Kirtland Air Force Base
Albuquerque, New Mexico
Attn: SWVSA

Commander
Headquarters Ground Electronics Engrg. Installation Agency
Griffiss Air Force Base
Rome, New York

Headquarters (10)
Armed Services Technical Information Agency
Arlington Hall Station
Arlington 12, Virginia
Attn: TIPCR
Via: Naval Weapons Lab.
Dahlgren, Va.
Attn: WH

Aerojet-General Corporation
P. O. Box 1947
Sacramento, California
Attn: R. W. Froelich, Dept. 6620
POLARIS Program

American Potash & Chemical Corp.
National Northern Division
P. O. Box 175
West Hanover, Mass.
Attn: Mr. J. A. Smith
Security Officer

National Aeronautics & Space Administration
Wallops Station
Wallops Island, Virginia
Attn: Head, Range Safety Section

DISTRIBUTION LIST (Continued)

Atlas Powder Company
Reynolds Ordnance Section
P. O. Box 271
Tamaqua, Penna.
Attn: Mr. R. McGirr

Bermite Powder Company
22116 West Soledad Canyon Road
Saugus, California
Attn: Mr. L. LoFiego

Chance Vought Corporation
P.O. Box 5907
Dallas, Texas
Attn: Mr. A. Latsko

Gruman Aircraft Engineering Corporation
Weapons Systems Department
Bethpage, Long Island, New York
Attn: Mr. E. J. Bonah

Librascope Division
General Precision, Inc.
670 Arques Avenue
Sunnyvale, California
Attn: Mr. R. Carroll Maninger

McCormick Selph Associates
Hollister, California
Attn: Technical Librarian

Midwest Research Institute
425 Volker Boulevard
Kansas City, Missouri
Attn: Security Officer

Mr. C. M. Fisher
RCA Service Company
Systems Engr. Facility
Government Service Dept.
838 N. Henry Street
Alexandria, Virginia

The Bendix Corp.
Scintilla Div.
Sidney, N.Y.
Attn: R. M. Purdy

Bethlehem Steel Company, CTD
97 E. Howard Street
Quincy, Massachusetts
Attn: Mr. W. C. Reid

The Franklin Institute
20th Street and Benjamin Franklin Parkway
Philadelphia 3, Pennsylvania
Attn: Mr. E. E. Hannum, Head
Applied Physics Laboratory

Jansky and Bailey, Inc.
1339 Wisconsin Avenue, N.W.
Washington, D. C.
Attn: Mr. F. T. Mitchell, Jr.
(Contract N178-7604

Lockheed Aircraft Corporation
P.O. Box 504
Sunnyvale, California
Attn: Missile Systems Div.,
Dept. 62-20
Mr. I. B. Gluckman
Attn: Missiles and Space Div.
Dept. 81-62
Mr. E. W. Tice
Attn: Missiles and Space Div.
Dept. 81-71
Mr. R. A. Fuhrman

Sandia Corporation (Division 1262)
Albuquerque, New Mexico
Via: FCDASA

University of Denver
Denver Research Institute
Denver 10, Colorado
Attn: Mr. R. B. Feagin

DISTRIBUTION (conclusion)

U.S. Flare Division Atlantic
Research Corp.
19701 W. Goodvale Road
Saugus, Calif.
Attn: Norman C. Eckert, Head,
R&D Group

North American Aviation, Inc.
Communications Services
4300 East 5th Ave.
Col. 16, Ohio

Chief
Defense Atomic Support Agency
Washington 25, D. C.
Attn: Major Melvin H. Johnsrud

W. L. Maxson Co.
475 Tenth Ave.
New York 18, N.Y.
Contract No. DA-28-017-ORD-4728

Aerojet-Genral Corporation
P.O. Box 296
Azusa, California
Attn: Myra Z. Grenier, Librarian

Welex Electronics Corp.
Solar Building, Suite 201
16th and K. Streets, N.W.
Washington 5, D. C.

Mr. D. S. Bassett
Support Equipment Department
Bldg. 6, Mail Station C1048
Hughes Aircraft Company
Culver City, California